Algorithm for the determination of a linear crack in an elastic body from boundary measurements

2010 Inverse Problems 26 085015

(http://iopscience.iop.org/0266-5611/26/8/085015)

Inverse Problems **26** (2010) 085015 (13pp) doi:10.1088/0266-5611/26/8/085015

Algorithm for the determination of a linear crack in an elastic body from boundary measurements

Elena Beretta[1], **Elisa Francini**[2], **Eunjoo Kim**[3] **and June-Yub Lee**[4,5]

[1] Dipartimento di Matematica G Calstelnuovo, Università di Roma La Sapienza, Italy
[2] Dipartimento di Matematica U Dini, Università di Firenze, Italy
[3] Institute of Mathematical sciences, Ewha Womans University, Seoul 120-750, Korea
[4] Department of Mathematics, Ewha Womans University, Seoul 120-750, Korea

E-mail: beretta@mat.uniroma1.it, francini@math.unifi.it, kej@ewha.ac.kr and jyllee@ewha.ac.kr

Received 1 March 2010, in final form 21 May 2010
Published 2 July 2010
Online at stacks.iop.org/IP/26/085015

Abstract
In this paper we consider the inverse problem of identifying a linear inclusion inside an elastic body from exterior boundary measurements. Based on the asymptotic formula by Beretta and Francini (2006 *SIAM J. Math. Anal.* **38** 1249–61), we design an effective reconstruction algorithm to find the endpoints and the thickness of a linear inclusion. Numerical experiments show that the algorithm is effective and stable.

1. Introduction

Let Ω be a bounded domain in $\mathbb{R}^2$ with smooth boundary and $\sigma = \sigma[P, Q] \subset \Omega$ be a line segment of the endpoints P and Q. We define D_ϵ to be a thin region surrounding σ with thickness ϵ,

$$D_\epsilon = \{x \in \Omega : d(x, \sigma) < \epsilon\}, \tag{1.1}$$

which represents a linear inclusion of a small thickness made of different elastic material from the surrounding medium.

Suppose that the elasticity tensor for $\Omega \setminus \overline{D_\epsilon}$ with the Lamé coefficients (λ_0, μ_0) is given by

$$(\mathbb{C}_0)_{ijk\ell} = \lambda_0 \delta_{ij}\delta_{k\ell} + \mu_0(\delta_{ik}\delta_{j\ell} + \delta_{i\ell}\delta_{jk}), \qquad i, j, k, \ell = 1, 2, \tag{1.2}$$

and let (λ_1, μ_1) be the Lamé coefficients for the linear inclusion D_ϵ; then the elasticity tensor for the whole domain can be written as follows:

$$\mathbb{C}_\epsilon = \mathbb{C}_0 \chi_{\Omega \setminus D_\epsilon} + \mathbb{C}_1 \chi_{D_\epsilon}. \tag{1.3}$$

[5] Author to whom any correspondence should be addressed.

Given a traction field g on $\partial\Omega$, the displacement field u_ϵ solves the following system:

$$\begin{cases} \operatorname{div}(\mathbb{C}_\epsilon \widehat{\nabla} u_\epsilon) = 0 & \text{in } \Omega, \\ (\mathbb{C}_\epsilon \widehat{\nabla} u_\epsilon)\nu = g, & \text{on } \partial\Omega, \\ \int_{\partial\Omega} u_\epsilon = 0, & \int_\Omega \nabla u_\epsilon - (\nabla u_\epsilon)^T = 0 \end{cases} \tag{1.4}$$

where $\widehat{\nabla} u = \frac{1}{2}(\nabla u + (\nabla u)^T)$ is the symmetric deformation tensor and ν denotes the outward unit normal to $\partial\Omega$. We denote by u_0 the background displacement field, namely the solution to

$$\begin{cases} \operatorname{div}(\mathbb{C}_0 \widehat{\nabla} u_0) = 0 & \text{in } \Omega, \\ (\mathbb{C}_0 \widehat{\nabla} u_0)\nu = g, & \text{on } \partial\Omega, \\ \int_{\partial\Omega} u_0 = 0, & \int_\Omega \nabla u_0 - (\nabla u_0)^T = 0. \end{cases} \tag{1.5}$$

Determining a homogeneous inclusion D_ϵ of small size from finitely many boundary measurements is an important problem arising in many applications, like nondestructive testing of materials and earth imaging. In [3] the authors deal with the problem of reconstructing diametrically small homogeneous elastic inclusions from boundary measurements. (Readers interested in theory and applications of this kind of inverse problems may refer [1, 7] and the references therein.)

We now move our attention to the inverse elastic problem of finding a thin linear elastic inclusion D_ϵ in $\Omega \subset \mathbb{R}^2$. Beretta and Francini suggested in [4] an asymptotic expansion formula for the boundary measurement $(u_\epsilon - u_0)|_{\partial\Omega}$ as follows:

$$(u_\epsilon - u_0)|_{\partial\Omega} = \epsilon w_\sigma(x) + o(\epsilon) \qquad \text{as} \quad \epsilon \to 0,$$

where the first-order asymptotic expansion term $w_\sigma(x)$ for some traction field g can be explicitly written in terms of the Neumann function $N_z(x)$ and the background solution u_0. This asymptotic expansion was used to derive in [5] Lipschitz continuous dependence of the segment σ from the boundary value of the correction term w_σ corresponding to a single measurement. In particular this implies that one single boundary measurement uniquely determines the position of the segment σ.

In section 3 we present two methods to detect the geometry of an inclusion. Both of the methods utilize the fact that $\epsilon w_\sigma(x)$, which can be easily computed by the boundary measurements $(u_\epsilon - u_0)|_{\partial\Omega}$, contains all the necessary information to reconstruct the linear inclusion parameters such as the endpoints P, Q and the thickness ϵ. A Newton-type iterative method is a direct application of the asymptotic formula; however, it fails in many cases. To overcome this difficulty, we propose a MUSIC-type elastic linear inclusion reconstruction (MELIR) algorithm which is based on a thorough study of a more explicit relationship between the term $\epsilon w_\sigma(x)$ and the inclusion parameters P, Q and ϵ. For this algorithm we use three different boundary measurements.

Numerical examples for both algorithms are presented in sections 3 and 4. Detailed characterization of the MELIR algorithm for a single inclusion has been discussed in subsections 4.2 and 4.3. The numerical stability under additive and multiplicative noise has been demonstrated in subsection 4.4 and generalization of the algorithm for a general shape of the domain has also been discussed in subsection 4.5.

2. Mathematical preliminaries

In this section we recall the definition and lemma in connection with the inverse problem of detecting a thin elastic inclusion from finitely many boundary measurements.

For $z \in \Omega$, the Neumann function denoted by $N_z(\cdot)$ is the solution to the following problem:

$$\begin{cases} \operatorname{div}(\mathbb{C}_0 \widehat{\nabla} N_z(\cdot)) = -\delta_z \mathrm{Id} & \text{in } \Omega, \\ (\mathbb{C}_0 \widehat{\nabla} N_z(\cdot))\nu = -\frac{1}{|\partial\Omega|}\mathrm{Id} & \text{on } \partial\Omega, \\ \int_{\partial\Omega} N_z = 0, & \int_\Omega \nabla N_z - (\nabla N_z)^T = 0, \end{cases} \tag{2.1}$$

where Id is the identity matrix in $\mathbb{R}^2$. Note that by well-known regularity results for elliptic systems, we have

$$N_z(x) = \Gamma_z(x) + \omega(x, z), \tag{2.2}$$

where ω is a smooth function of x and z and $\Gamma_z(x) := \Gamma(x - z)$ is the fundamental free space solution of $\operatorname{div}(\mathbb{C}_0 \widehat{\nabla} \cdot)$, given by

$$\Gamma_{ij}(y) = \frac{A}{2\pi}\delta_{ij} \log|y| - \frac{B}{2\pi}\frac{y_i y_j}{|y|^2}, \qquad i, j = 1, 2, \tag{2.3}$$

with

$$A = \frac{1}{2}\left(\frac{1}{\mu_0} + \frac{1}{2\mu_0 + \lambda_0}\right) \qquad \text{and} \qquad B = \frac{1}{2}\left(\frac{1}{\mu_0} - \frac{1}{2\mu_0 + \lambda_0}\right).$$

The following lemma (see [3]), that relates the fundamental solution with the Neumann function, is useful for the computation of the Neumann function in the reconstruction procedure. Before stating the lemma, we define Ψ to be the vector space of all homogeneous linear solutions of the equations $\operatorname{div}(\mathbb{C}_0 \widehat{\nabla} u) = 0$ in Ω and such that $(\mathbb{C}_0 \widehat{\nabla} u)\nu = 0$ on $\partial\Omega$, and, for a simply connected Lipschitz domain D compactly contained in Ω we define $\Psi^*(\partial D) := \{f \in L^2(\partial D) : \int_{\partial D} f \cdot \psi \, \mathrm{d}\sigma = 0 \text{ for all } \psi \in \Psi\}$.

Lemma 2.1. *For $z \in \Omega$ and $x \in \partial\Omega$, let $\Gamma_z(x)$ and $N_z(x)$ be the fundamental and the Neumann function with a point source at z, respectively. Then*

$$\left(-\tfrac{1}{2} + \mathcal{K}_\Omega\right) N_z(x) = \Gamma_z(x) \qquad \mod \Psi \tag{2.4}$$

or to be more precise, for any simply connected Lipschitz domain D compactly contained in Ω and for any $g \in \Psi^*(\partial D)$, we have

$$\int_{\partial D} \left(\frac{1}{2}I + \mathcal{K}_\Omega\right) N_z(x) g(z) \, \mathrm{d}\sigma_z = \int_{\partial D} \Gamma_z(x) g(z) \, \mathrm{d}\sigma_z, \qquad x \in \partial\Omega. \tag{2.5}$$

It is worth remarking that solving equation (2.5) numerically is much easier than solving the integral equation for a forward solver. Since the source points $z \in \partial D$ are well separated from the target points $x \in \partial\Omega$, the integral kernel $\left(\frac{1}{2}I + \mathcal{K}_\Omega\right)$ is a smooth operator and thus the numerical procedure to compute N_z converges in a few iterations. It is a great advantage that our MELIR algorithm (presented in section 3.2) does not use an iterative forward solver but requires only numerical evaluations of the Neumann functions.

We now move our attention to a more specific problem with a thin linear elastic inclusion D_ϵ in $\Omega \subset \mathbb{R}^2$. The following lemma (see [5]) gives an asymptotic expansion for $(u_\epsilon - u_0)|_{\partial\Omega}$ as $\epsilon \to 0$ with the traction field g on $\partial\Omega$ of the following form:

$$g = (\mathbb{C}_0 W)\nu, \tag{2.6}$$

where W is a non-zero symmetric 2×2 matrix.

Lemma 2.2. *For a given line segment $\sigma = \sigma[P, Q]$ with the tangent direction vector $\tau = \frac{Q-P}{||Q-P||}$, let u_ϵ be the solution of (1.4) with a thin linear inclusion D_ϵ corresponding to a traction field of the form $g = (\mathbb{C}_0 W)\nu$. For $x \in \partial\Omega$,*

$$(u_\epsilon - u_0)(x) = \epsilon w_\sigma(x) + o(\epsilon). \tag{2.7}$$

Here w_σ is defined by

$$w_\sigma(x) = \int_\sigma \mathbb{C}_0 \widehat{\nabla} N_z(x)\nu \cdot \varphi \, d\sigma_z + \frac{(N_Q(x) - N_P(x)) \cdot (Q - P)}{||Q - P||} f \tag{2.8}$$

where φ is a vector whose components in the (ν, τ) directions are given by

$$\varphi \cdot \nu = \frac{2}{\lambda_1 + 2\mu_1}((\lambda_1 - \lambda_0)\,\mathrm{tr}(W) + 2(\mu_1 - \mu_0)\nu^T W \nu), \tag{2.9}$$

$$\varphi \cdot \tau = \frac{4(\mu_1 - \mu_0)}{\mu_0}\nu^T W \tau, \tag{2.10}$$

and f is the scalar constant function

$$f = \alpha\,\mathrm{tr}(W) - \beta\nu^T W \nu \tag{2.11}$$

with α and β given by

$$\alpha = \frac{4}{\lambda_1 + 2\mu_1}((\mu_1 - \mu_0)(\lambda_1 + 2\mu_1) + \mu_1(\lambda_1 - \lambda_0)) \quad \text{and} \quad \beta = \frac{8(\mu_1 - \mu_0)}{\lambda_1 + 2\mu_1}(\lambda_1 + \mu_1).$$

The lemma shows that the perturbation function $w_\sigma(x)$ consists of an integral of the Neumann function and a part explicitly depending on P and Q. In the next section we use this result in order to find the endpoints and the thickness of a thin linear inclusion.

The previous result shows that the boundary measurement contains enough information on the inclusion. As a matter of fact, the following lemma (from [5]) states that one boundary measurement is enough to distinguish two different linear inclusions.

Lemma 2.3. *Let σ_0 and σ_1 be two segments contained in Ω; let w_{σ_0} and w_{σ_1} be the correction terms given by (2.8) and corresponding to the same traction g; then*

$$d_{\mathcal{H}}(\sigma_0, \sigma_1) \leqslant C \left\| w_{\sigma_0} - w_{\sigma_1} \right\|_{L^2(\Gamma)}$$

where $d_{\mathcal{H}}$ denotes the Hausdorff distance and Γ is an open portion of $\partial\Omega$.

3. A MUSIC-type reconstruction (MELIR) algorithm

In this section we apply the asymptotic formula ((2.7) and (2.8)) to design a MUSIC (MUltiple SIgnal Classification)-type algorithm for the reconstruction of a single thin linear inclusion from a finite number of boundary measurements. (Readers interested in the MUSIC-type algorithms can refer to [2, 6, 8, 12].)

Before presenting a MELIR algorithm, we start with a Newton-type algorithm as a direct application of the asymptotic formula. For a given traction g, let u_ϵ and u_0 be the solution of the elastic problem (1.4) with and without inclusion, respectively. Define the map Λ_ϵ by

$$\Lambda_\epsilon(g) = u_\epsilon|_{\partial\Omega}. \tag{3.1}$$

In order to use lemma 2.2, we choose Neumann data of the form

$$g_j = (\mathbb{C}_0 W_j)\nu, \qquad j = 1, \ldots, 3 \tag{3.2}$$

where

$$W_1 := \begin{pmatrix} 1 & 0 \\ 0 & 0 \end{pmatrix}, \qquad W_2 := \begin{pmatrix} 0 & 1 \\ 1 & 0 \end{pmatrix}, \qquad W_3 := \begin{pmatrix} 0 & 0 \\ 0 & 1 \end{pmatrix} \tag{3.3}$$

are a basis in the space of 2×2 symmetric matrices.

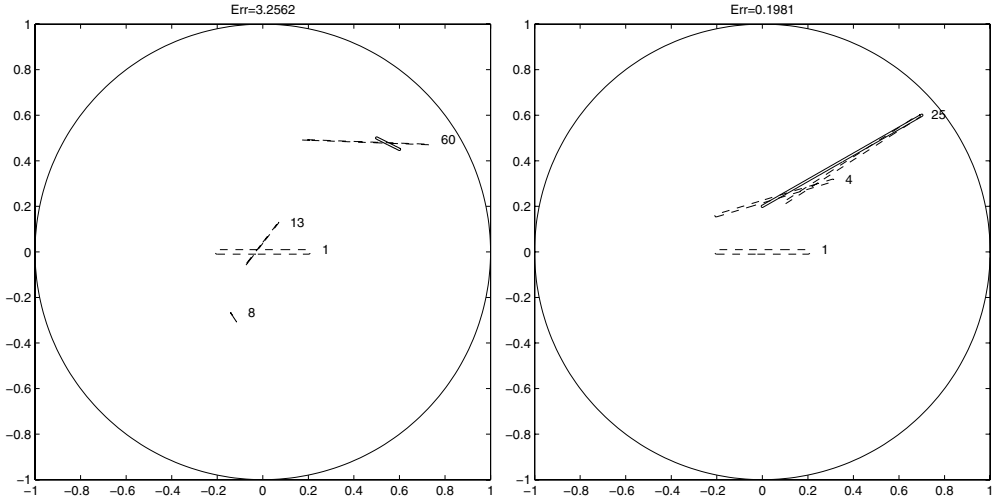

Figure 1. Numerical results of Newton iteration for two cases. Solid lines show the actual inclusions and dotted lines with iteration counter show some of computed results.

3.1. A Newton-type search method

For a given boundary measurement $(\Lambda_\epsilon - \Lambda_0)(g_j)$ on $\partial\Omega$, one may define an error functional F_{g_j} as a function of P, Q and ϵ:

$$F_{g_j}(P, Q, \epsilon) := \left\| (\Lambda_\epsilon - \Lambda_0)(g_j) - \epsilon w_\sigma^{g_j} \right\|_{L^2(\partial\Omega)} \tag{3.4}$$

where $\sigma := [P, Q]$ and $w_\sigma^{g_j}$ is the first-order asymptotic expansion term defined in (2.8) of lemma 2.2. Since F_{g_j} depends on the two endpoints P, Q and the thickness ϵ, it is a natural idea to use a Newton-type iterative method as proposed in [11]. A direct application of the lemma for the detection of a thin linear inclusion would be a Newton-type method as follows:

$$\min_{P,Q,\epsilon} \sum_{j=1}^{3} \left| F_{g_j}(P, Q, \epsilon) \right|^2 \tag{3.5}$$

for given boundary measurements g_j and $\Lambda_\epsilon(g_j)$ for $j = 1, \ldots, 3$.

Figure 1 shows the results of the Newton iteration for two different configurations. The first case with $P = (0.5, 0.5)$, $Q = (0.6, 0.45)$, $\epsilon = 0.005$ did not converge for the first 60 Newton iterations. The second case $P = (0.0, 0.2)$, $Q = (0.7, 0.6)$, $\epsilon = 0.005$ converges but with rather large relative error, Err $= 0.1981$ even after 25 iterations. (Details of the numerical computation can be found in section 4.) The Newton method may and may not converge to the original domain depending on the shape of the domain and the initial guess. The Newton iteration fails in many cases because the minimal function F is not a simple convex function and P, Q and ϵ are not well separated in F.

Figure 2 shows the structure of F near the actual endpoints and the thickness of the thin linear inclusion and explains why the Newton iteration is not successful in many cases. The three-dimensional plots in figure 2 show the shape of F as a function of P, Q and ϵ in the neighborhood of the actual data. For convenience, we plot the values of $F(P, Q, \epsilon)$ as functions of two variables, x-coordinates of P and ϵ, while the y-coordinates of P and Q are fixed to the actual data. The Newton iteration fails in many cases because F has a quite complicated structure globally even though $F(P, Q, \epsilon)$ has a local minimum near the actual parameters of the thin linear inclusion. In order to overcome this difficulty, we propose a new

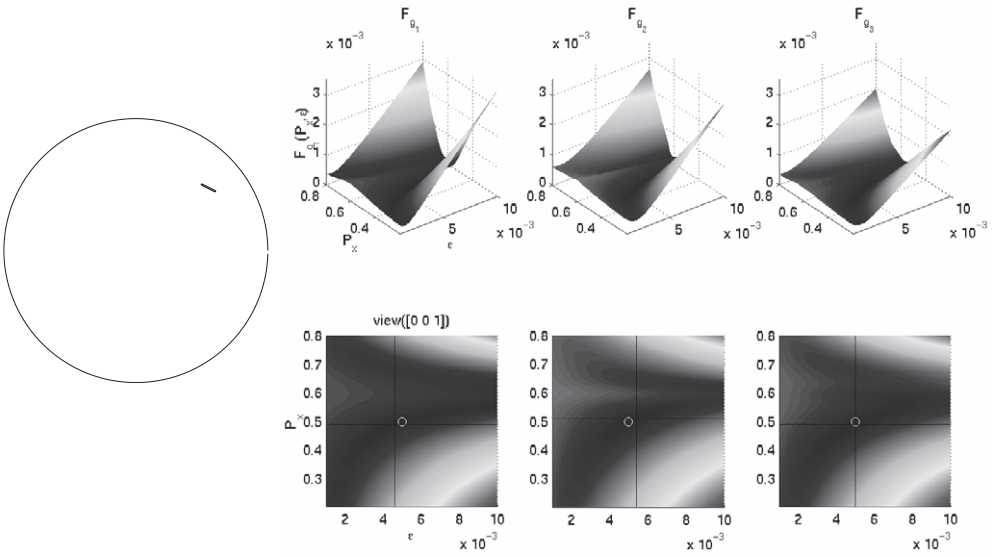

Figure 2. Newton minimizer function. The figure on the left shows the actual domain. The 3D and 2D plots on the right illustrate $F_{g_j}(P_x, \epsilon)$ for Neumann data g_j, $j = 1, 2, 3$. The intersection of two lines in the plots at the bottom is the actual point, and the circle is the computational minimal point of F_{g_j}.

MUSIC-type numerical algorithm which utilizes the asymptotic formula ((2.7) and (2.8)) for the detection of the endpoints and the thickness in a stable manner.

3.2. A MUSIC-type elastic linear inclusion reconstruction

The MELIR algorithm first computes the endpoints P, Q of an inclusion using three measured data, $(\Lambda_\epsilon - \Lambda_0)(g_j)|_{\partial\Omega}$ for $j = 1, 2, 3$. Once the endpoints are detected, the thickness ϵ can be easily recovered from (2.7) using the ratio between $||(\Lambda_\epsilon - \Lambda_0)(g_j)||_{L^2(\partial\Omega)}$ and $\left\| w_\sigma^{g_j} \right\|_{L^2(\partial\Omega)}$.

For the sake of simplicity, we take Ω to be the unit disk centered at zero and choose N equi-spaced points y_i along the boundary $\partial\Omega$, say $\{(\cos\theta_i, \sin\theta_i) : \theta_i = 2\pi(i-1)/N, i = 0, 1, \ldots, N-1\}$. Suppose that the $N \times 3$ matrix $A := \left(w_\sigma^{g_j}(y_i)\right)$ has the spectral decomposition

$$A = \sum_{p=1}^{3} \sigma^p u^p \otimes v^p, \tag{3.6}$$

where σ^p are the singular values of A, and u^p, v^p are the corresponding singular vectors. Let $\mathbb{P} : \mathbb{R}^N \longrightarrow \text{span}\{u^1, u^2, u^3\}$ be the orthogonal projector $\mathbb{P} = \sum_{p=1}^{3} u^p \otimes u^p$.

The most important observation to derive a MUSIC-type algorithm is that the second part of the asymptotic expansion term of (2.8) $\frac{(N_Q - N_P)\cdot(Q-P)}{||Q-P||}$ lies in the space spanned by columns of A. The following lemma formalizes the observation.

Lemma 3.1. *Suppose P, Q are the endpoints of a thin inclusion. Then we have* $\frac{(N_Q - N_P)\cdot(Q-P)}{||Q-P||} \in \text{span}\{u^1, u^2, u^3\}$ *or equivalently*

$$(I - \mathbb{P})\left(\frac{(N_Q - N_P)\cdot(Q-P)}{||Q-P||}\right) = 0. \tag{3.7}$$

Proof. Let $g = (\mathbb{C}_0 W)\nu$ be the Neumann data corresponding a symmetric matrix $W = \left(\begin{smallmatrix} a & b \\ b & c \end{smallmatrix}\right)$. Since $\sigma := [P, Q]$ is a straight line segment, φ is a constant vector in (2.8); thus, the first-order expansion term $w_\sigma(x)$ can be written as follows:

$$w_\sigma(x) = (\varphi \cdot \nu) \int_\sigma \mathbb{C}_0 \widehat{\nabla} N_z(x)\nu \cdot \nu \, d\sigma_z + (\varphi \cdot \tau) \int_\sigma \mathbb{C}_0 \widehat{\nabla} N_z(x)\nu \cdot \tau \, d\sigma_z + f(N_Q - N_P)(x) \cdot \tau. \tag{3.8}$$

Here all the three coefficients, $\varphi \cdot \nu$, $\varphi \cdot \tau$ and f are linear functions with respect to a, b, c. Put $\ell_1 := \frac{\lambda_1 - \lambda_0}{\mu_1 - \mu_0}$ and $\ell_2 := \frac{\lambda_1}{\mu_1}$. From the relation $\tau = \pm\binom{-\nu_2}{\nu_1}$, it follows that

$$\begin{pmatrix} \frac{\lambda_1 + 2\mu_1}{2(\mu_1 - \mu_0)} \varphi \cdot \nu \\ \frac{\mu_0}{4(\mu_1 - \mu_0)} \varphi \cdot \tau \\ \frac{\lambda_1 + 2\mu_1}{4\mu_1(\mu_1 - \mu_0)} f \end{pmatrix} = M \begin{pmatrix} a \\ b \\ c \end{pmatrix}$$

where M is the 3×3 matrix defined by

$$M = \begin{pmatrix} \ell_1 + 2\nu_1^2 & 4\nu_1\nu_2 & \ell_1 + 2\nu_2^2 \\ \mp\nu_1\nu_2 & \pm\left(\nu_1^2 - \nu_2^2\right) & \pm\nu_1\nu_2 \\ (\ell_1 + 1) + (\ell_2 + 1)\left(1 - 2\nu_1^2\right) & -4(\ell_2 + 1)\nu_1\nu_2 & (\ell_1 + 1) + (\ell_2 + 1)\left(1 - 2\nu_2^2\right) \end{pmatrix}.$$

As can be seen in [5] (proof of lemma 4.1), if $\ell_1 > 0$ and $\ell_2 > 0$, we can derive $\det(M) = \pm 2(\ell_1 + 1)(\ell_2 + 2) \neq 0$, and always find a non-zero matrix W satisfying $\varphi \cdot \nu = 0$, $\varphi \cdot \tau = 0$ and $f \neq 0$. For such a Neumann data $g = (\mathbb{C}_0 W)\nu$, $w_\sigma(x)$ becomes $f(N_Q - N_P)(x) \cdot \tau$. Then

$$(N_Q - N_P)(y_i) \cdot \tau \in \operatorname{span}\{u^1, u^2, u^3\}, \tag{3.9}$$

which completes the proof. □

Remark 3.2. For the present reconstruction algorithm, a two-dimensional subspace of $\operatorname{span}\{u^1, u^2, u^3\}$ is enough to guarantee both coefficients of the integral $\varphi \cdot \nu$, $\varphi \cdot \tau$ to be zero simultaneously; therefore, one can conclude that two measurements are almost always enough. However we use all three independent basis functions $\{u^1, u^2, u^3\}$ of arbitrary symmetric Neumann data $g = (\mathbb{C}_0 W)\nu$ in the proof of the lemma and the implementation of the MELIR numerical algorithm for the sake of simplicity.

Let $A_\epsilon := ((\Lambda_\epsilon - \Lambda_0)(g_j)(y_i))$. The $N \times 3$ matrix A_ϵ has a spectral decomposition

$$A_\epsilon = \sum_{p=1}^{3} \sigma_\epsilon^p u_\epsilon^p \otimes v_\epsilon^p,$$

where σ_ϵ^p are the singular values of A_ϵ, and u_ϵ^p, v_ϵ^p are the corresponding singular vectors. Let $\mathbb{P}_\epsilon : \mathbb{R}^N \longrightarrow \operatorname{span}\left\{u_\epsilon^1, u_\epsilon^2, u_\epsilon^3\right\}$ be the orthogonal projector $\mathbb{P}_\epsilon = \sum_{p=1}^3 u_\epsilon^p \otimes u_\epsilon^p$.

We do not have A as our data. Note that A_ϵ can be computed from boundary measurements. Lemma 2.2 shows that A_ϵ is an approximation of A. In order to find the endpoints of the thin inclusion, we seek to find those points, P and Q, minimizing

$$L(P, Q) := \frac{\left\| (I - \mathbb{P}_\epsilon) \left(\frac{(N_Q - N_P) \cdot (Q - P)}{\|Q - P\|} \right) \right\|_{L^2(\partial\Omega)}}{\left\| \mathbb{P}_\epsilon \left(\frac{(N_Q - N_P) \cdot (Q - P)}{\|Q - P\|} \right) \right\|_{L^2(\partial\Omega)}}$$

where the Neumann function N_z is computed using lemma 2.1. The reconstruction algorithm can be summarized as follows.

[The MELIR algorithm]

Step 1. Measure Dirichlet data $(\Lambda_\epsilon - \Lambda_0)(g)$ on $\partial\Omega$ for Neumann with data $g_j = (\mathbb{C}_0 W_j)\nu$ with

$$W_1 := \begin{pmatrix} 1 & 0 \\ 0 & 0 \end{pmatrix}, \qquad W_2 := \begin{pmatrix} 0 & 1 \\ 1 & 0 \end{pmatrix}, \qquad W_3 := \begin{pmatrix} 0 & 0 \\ 0 & 1 \end{pmatrix}. \tag{3.10}$$

Then form the $N \times 3$ matrix

$$A_\epsilon = ((\Lambda_\epsilon - \Lambda_0)(g_j)(y_i))$$

for $y_i \in \partial\Omega$, $i = 1, \ldots, N$, and $j = 1, 2, 3$.

Step 2. Compute the singular value decomposition of the matrix A_ϵ. Let σ_ϵ^p be the singular values of A_ϵ, and u_ϵ^p, v_ϵ^p be the corresponding singular vectors. Then A_ϵ has the spectral decomposition

$$A_\epsilon = \sum_{p=1}^{3} \sigma_\epsilon^p u_\epsilon^p \otimes v_\epsilon^p. \tag{3.11}$$

Define an orthogonal projection operator $\mathbb{P}_\epsilon : \mathbb{R}^N \to \text{span}\{u_\epsilon^1, \ldots, u_\epsilon^3\}$, $\mathbb{P}_\epsilon = \sum_{p=1}^{3} u_\epsilon^p \otimes u_\epsilon^p$ and a minimization functional $L(P,Q)$ by

$$L(P, Q) := \frac{\left\| (I - \mathbb{P}_\epsilon)\left(\frac{(N_Q - N_P)\cdot(Q-P)}{\|Q-P\|} \right) \right\|_{L^2(\partial\Omega)}}{\left\| \mathbb{P}_\epsilon \left(\frac{((N_Q - N_P))\cdot(Q-P)}{\|Q-P\|} \right) \right\|_{L^2(\partial\Omega)}}, \tag{3.12}$$

where the Neumann function N_z is computed using lemma 2.1. Then compute the endpoints P^c and Q^c which minimize $L(P,Q)$.

Step 3. Using the computed endpoints, P^c and Q^c at step 2, find the thickness ϵ^c using the ratio between $(\Lambda_\epsilon - \Lambda_0)(g)$ and $\omega_{\sigma^c}^g$ for any Neumann data g:

$$\epsilon^c = \frac{\|(\Lambda_\epsilon - \Lambda_0)(g)\|_{L^2(\partial\Omega)}}{\left\| \omega_{\sigma^c}^g \right\|_{L^2(\partial\Omega)}} \tag{3.13}$$

where $\sigma^c := [P^c, Q^c]$ is a line segment joining P^c and Q^c. There is no extra cost to compute $(\Lambda_\epsilon - \Lambda_0)(g)$ for any symmetric traction field since it is a just linear combination of the given solutions, $(\Lambda_\epsilon - \Lambda_0)(g_j)$, $j = 1, 2, 3$. In our experiments, we select $g = \mathbb{C}_0 \left(\begin{smallmatrix} 2 & 0 \\ 0 & -1 \end{smallmatrix}\right)\nu$ as Neumann data.

4. Numerical experiments and discussions

In this section, we show some numerical experiments of reconstruction of a single thin inclusion using the MELIR algorithm. In the computations the background domain Ω is assumed to be the unit disk centered at the origin, and the inclusion D_ϵ is a thin. We reconstruct the thin inclusion only using the boundary measurements without the knowledge of the interior Lamé constants. If P^c, Q^c and ϵ^c are the detected endpoints and thickness, we define the error Err as follows:

$$\text{Err} := \sqrt{\frac{||P - P^c||^2 + ||Q - Q^c||^2}{||P - Q||^2} + \frac{|\epsilon - \epsilon^c|^2}{\epsilon^2}}. \tag{4.1}$$

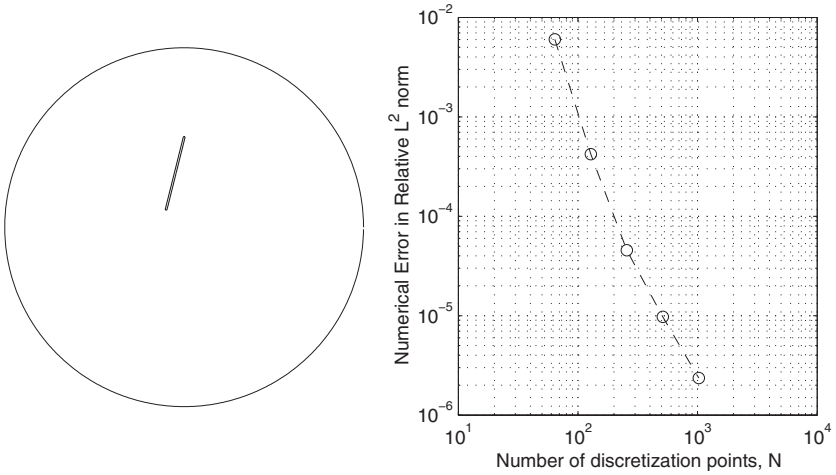

Figure 3. Convergence error of the forward solver with $N = 64$–1024 for the domains with thin inclusion D_ϵ. The diagram on the right shows the convergence errors of u_ϵ on $\partial\Omega$.

4.1. A forward solver

We implement an integral equation solver in FORTAN in order to generate forward solutions of problem (1.4). Single- and double-layer potentials have been numerically evaluated using the trapezoidal rule with equally spaced discretization points along the interface and a generalized minimum residual (GMRES) method has been used to solve the system of integral equations. Readers interested in the forward solver may find a more detailed description in a previous paper [9, 10]. We compute the forward solutions u_ϵ with $N = 64, 128, 25, 512, 1024$ equi-spaced points on ∂D_ϵ, and $N/4$ points on $\partial\Omega$. And then they are compared with the solutions on the finer grid with $N = 2048$. Figure 3 shows the convergence of a forward solver as a function of discretization points N for the computational domain with one linear inclusion of $P = (-0.1, 0.1)$, $Q = (0.0, 0.5)$ $\epsilon = 0.005$.

The numerical computation shows that the forward integral equation solver achieves third-order convergence. We set $N = 1024$ for all the simulation experiments (except otherwise noted) in this section, which gives around five digits of accuracy. We also fix the Lamé parameters for the inclusions in this section to $(\lambda_1, \mu_1) = (6, 9)$ while the background parameters are $(\lambda_0, \mu_0) = (4, 6)$.

4.2. Reconstruction of a single inclusion

In this subsection, we reconstruct a thin linear inclusion using the MELIR algorithm presented in section 3.2. For the simulation in this subsection, three forward solutions for g_j, $j = 1, 2, 3$, are computed using the forward solver described in the previous subsection. Then a simple minimization method using the subplx routine from the Netlib repository has been applied to get the minimal points P^c, Q^c in (3.12). Table 1 and figure 4 summarize the computational results for four different computational domains. The results show that the MUSIC-type method detects the thin inclusion pretty well (with around a few percent of relative error).

Both the Newton method and the MELIR algorithm utilize the same expansion formula ((2.7) and (2.8)); however, the Newton method is far less stable than the MELIR algorithm.

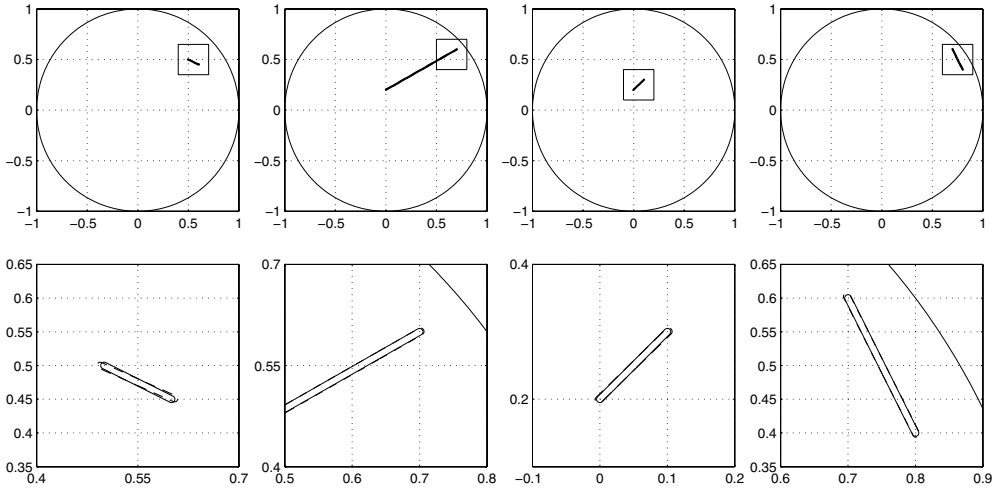

Figure 4. Reconstruction results of the MELIR algorithm. The solid line represents the actual domains and the dashed lines represent the computed results. The figures at the bottom are 6.67 times zoom up of the corresponding results.

Table 1. Computational domain and reconstruction error.

Case	P	Q	ϵ	$\frac{\|\|P-P^c\|\|}{\|\|P-Q\|\|}$	$\frac{\|\|Q-Q^c\|\|}{\|\|P-Q\|\|}$	$\frac{\|\epsilon^c-\epsilon\|}{\epsilon}$	Err
1	(0.5,0.5)	(0.6,0.45)	5.0×10^{-3}	0.050	0.042	0.070	0.0964
2	(0.0,0.2)	(0.7,0.6)	5.0×10^{-3}	0.002	0.002	0.057	0.0574
3	(0.0,0.2)	(0.1,0.3)	5.0×10^{-3}	0.013	0.013	0.053	0.0558
4	(0.7,0.6)	(0.8,0.4)	5.0×10^{-3}	0.013	0.009	0.008	0.0178

Unstable behavior of the Newton method is perhaps due to the fact that the minimizer F is not a simple convex function as shown in figure 2 and the method is to detect the thickness and the endpoints all together. On the other hand, the MUSIC-type first finds the endpoints using more explicit formula (3.12) and computes the thickness later. It is also worth remarking that the reconstruction method does not require to know the Lamé constants of inclusion. Using only the exterior boundary measurements and the background Lamé constants, we obtain near-perfect results.

4.3. Reconstruction with a thicker inclusion

The MELIR algorithm strongly depends on the asymptotic formula (2.7) for a small thickness $\epsilon \ll 1$. Thus the computational results may not be accurate if the thickness becomes too large. The following experimentation shows the computational error as a function of ϵ. We fix all other parameters such as the endpoints $P = (-0.4, 0.1)$, $Q = (-0.3, 0.5)$, and Lamé parameters.

Figure 5 shows the computational domains (with inclusion of various thickness) and the reconstruction error. As guessed, the reconstruction error becomes larger as the thickness grows. The growth of error for $\epsilon \leqslant 3 \times 10^{-3}$ is due to the lack of numerical accuracy for the forward solver with a fixed number of discretization points.

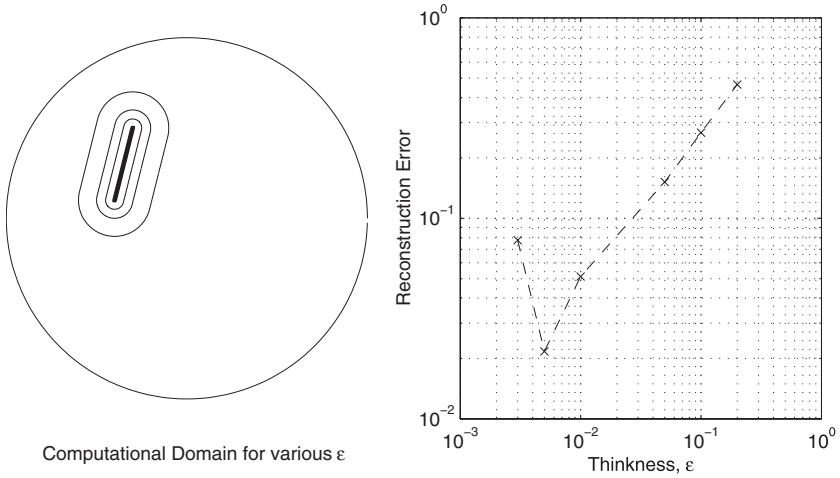

Figure 5. Reconstruction results in case that the thickness of inclusion is not thin.

4.4. Numerical stability of the reconstruction algorithm

The MELIR algorithm depends only on the boundary perturbation, $A_{ij} = (\Lambda_\epsilon - \Lambda_0)(g_j)(x_i)$ for $i = 1, \ldots, N$, $j = 1, 2, 3$. In this example, we check the numerical stability of the algorithm by perturbing the measured data on the boundary. The multiplicative noise simulates the error on data collection,

$$A_{ij}^{\mathrm{MUL}} = A_{ij} \cdot (1 + NL \cdot N(0, 1)), \tag{4.2}$$

and the additive noise does the effect of white background noise:

$$A_{ij}^{\mathrm{ADD}} = A_{ij} + NL \cdot N(0, 1) \cdot ||(\Lambda_\epsilon - \Lambda_0)(g_j)||_{L^2(\partial\Omega)}, \tag{4.3}$$

where NL denotes the noise level and $N(0, 1)$ denotes the Gaussian distribution with $\mu = 0, \sigma = 1$.

We add two different types of error described above to the simulation data one at a time and compare the reconstructed values with the actual parameters. Figure 6 shows the computational domain and the reconstruction error as a function of the noise level. The reconstruction error depends linearly on the noise level and we conclude that the MELIR algorithm has linear stability with respect to the multiplicative and the additive noise.

4.5. Comments on generalization

Our final examples illustrate the behavior of the MELIR algorithm for a computational domain with multiple inclusions. Figure 7 shows the six computational results for domains with general shape inclusions. The first domain contains a single inclusion of *S*-shape and the domains of the rest cases consist of multiple thin linear inclusions.

Although the MELIR algorithm has been developed for a domain with a single inclusion of linear shape, we believe from the various numerical simulations that it generates a reasonably good approximated shape even for the domain with multiple inclusions. More details on the characteristics of the algorithm depending on the shape and the material parameters of the inclusions will be studied in near future.

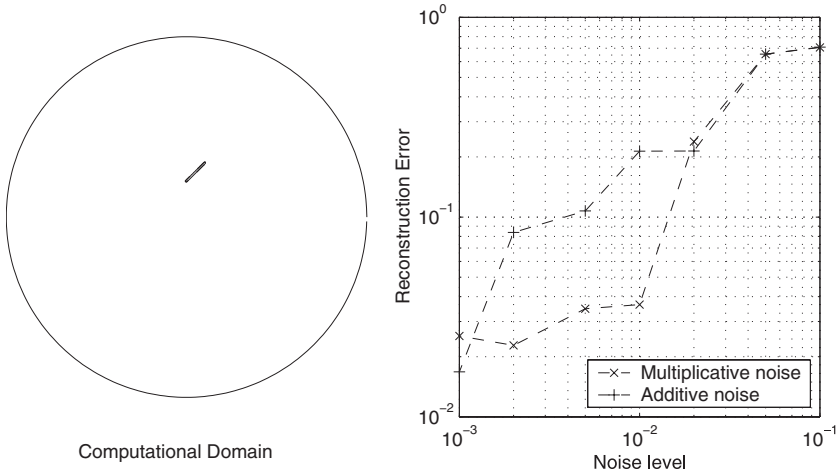

Figure 6. Reconstruction results in the case when the thickness of inclusion is not thin.

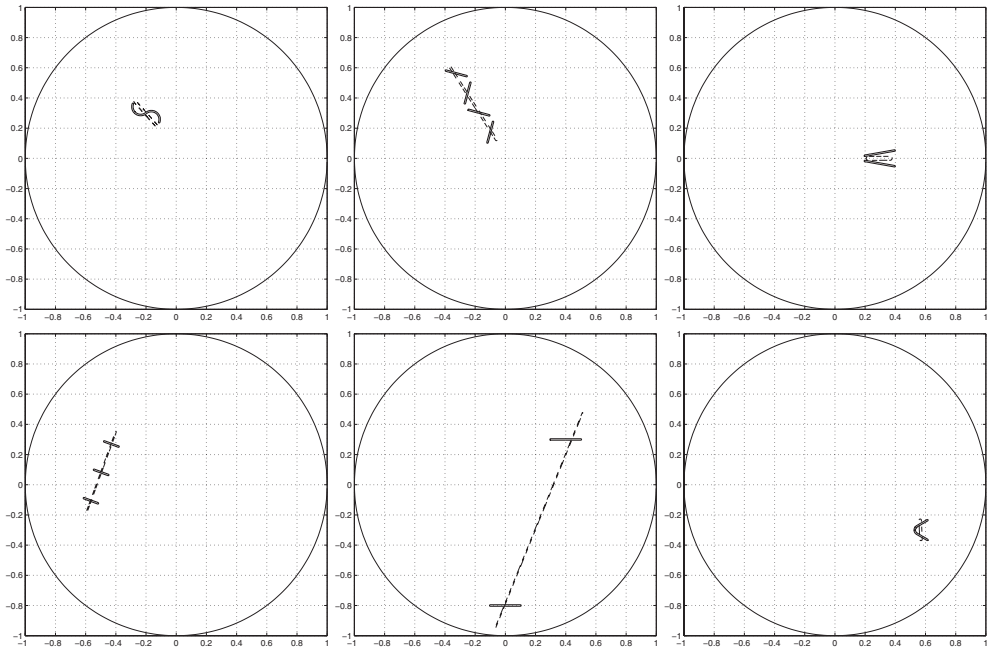

Figure 7. Reconstruction results with several inclusions.

Acknowledgments

EB was partially supported by MIUR under grant 20089PWTPS. EF was partially supported by MIUR under grant 20089PWTPS. EK was supported by the Korea Research Foundation (KRF-2008-359-C00004). JYL was supported by the Priority Research Centers Program through the National Research Foundation of Korea (NRF-2009-0093827).

References

[1] Ammari H and Kang H 2004 *Reconstruction of Small Inhomogeneities from Boundary Measurements (Lecture Notes in Mathematics* vol 1846*)* (Berlin: Springer)

[2] Ammari H, Kang H, Kim E, Louati K and Vogelius M 2008 A MUSIC-type algorithm for detecting internal corrosion from electrostatic boundary measurements *Numer. Math.* **108** 501–28

[3] Ammari H, Kang H, Nakamura G and Tanuma K 2002 Complete asymptotic expansions of solutions of the system of elastic in the presence of an inclusion of small diameter and detection of aninclusion *J. Elast.* **67** 97–129

[4] Beretta E and Francini E 2006 An asymptotic formula for the displacement field in the presence of thin elastic inhomogeneities *SIAM J. Math. Anal.* **38** 1249–61

[5] Beretta E, Francini E and Vessella S 2008 Determination of a linear crack in an elastic body from boundary measurements—Lipschitz stability *SIAM J. Math. Anal.* **40** 984–1002

[6] Cheney M 2001 The linear sampling method and the MUSIC algorithm *Inverse Problems* **17** 591–5

[7] Colton D and Kress R 1998 *Inverse Acoustic and Electromagnetic Scattering Theory* 2nd edn (Berlin: Springer)

[8] Devaney A J, Marengo E A and Gruber F K 2005 Timereversal-based imaging and inverse scattering of multiply scattering point targets *J. Acoust. Soc. Am.* **118** 3129–38

[9] Kang H, Kim E and Lee J-Y 2003 Identification of elastic inclusions and elastic moment tensors by boundary measurements *Inverse Problems* **19** 703–24

[10] Kang H, Kim E and Lee J-Y 2007 Numerical reconstruction of a cluster of small elastic inclusions *Inverse Problems* **23** 2311–24

[11] Kress R 1998 *Numerical Analysis* (New York: Springer)

[12] Kirsch A 2002 The MUSIC-algorithm and the factorization method in inverse scattering theory for inhomogeneous media *Inverse Problems* **18** 1025–40